iScience

Article

Application of spatial transcriptomics across organoids for a high-resolution, spatial whole-transcriptome benchmarking dataset

Graphical abstract

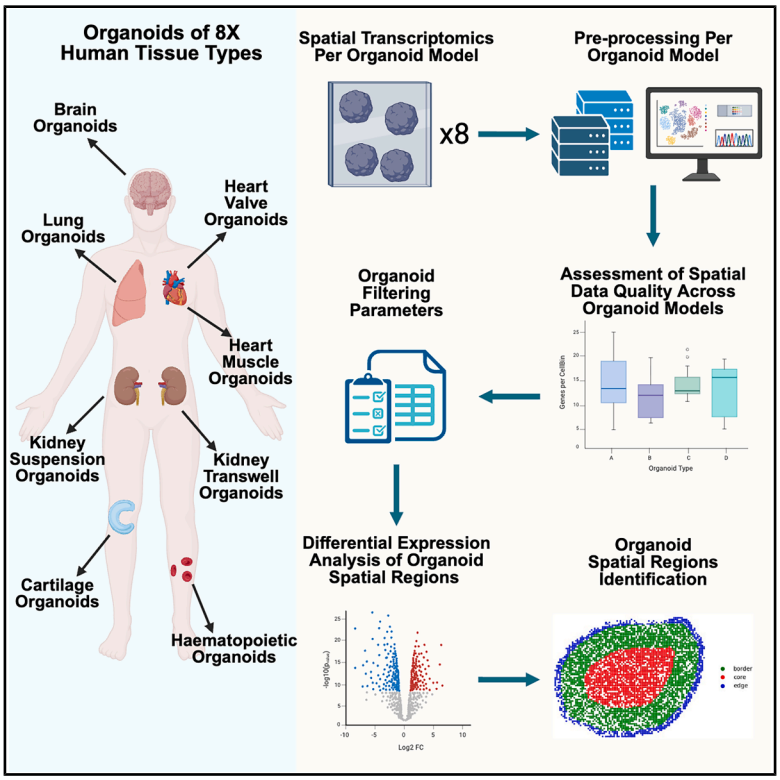

Highlights

- Parallel spatial transcriptomics profiling of 8 stem cell-derived organoid models
- Stereo-seq assay optimization for profiling of multiple organoid types
- Placement of multiple organoids of the same tissue on a single Stereo-seq chip
- New computational method to partition organoids regions for spatial profiling

Authors

Maria Rosaria Nucera, Natalie Charitakis, Ryan F. Leung, ..., Silvia Velasco, Fernando J. Rossello, Mirana Ramialison

Correspondence

david.elliot@mcri.edu.au (D.A.E.), enzo.porello@mcri.edu.au (E.R.P.), maree.faux@mcri.edu.au (M.C.F.), david.eisenstat@mcri.edu.au (D.D.E.), silvia.velasco@mcri.edu.au (S.V.), fernando.rossello@mcri.edu.au (F.J.R.), mirana.ramialison@mcri.edu.au (M.R.)

In brief

Health sciences; Medicine; Bioinformatics

Nucera et al., 2026, iScience *29*, 115827
June 19, 2026
https://doi.org/10.1016/j.isci.2026.115827

CellPress

iScience

CellPress
OPEN ACCESS

Article

Application of spatial transcriptomics across organoids for a high-resolution, spatial whole-transcriptome benchmarking dataset

Maria Rosaria Nucera,[1,2,3,15] Natalie Charitakis,[1,2,3,15] Ryan F. Leung,[1,2,3,15] Anna Leichter,[1,2] Natasha K. Tuano,[1,2,3] Marzena Walkiewicz,[1,2] Vallari Sawant,[1,2,3] Lynn Rowley,[1,2] Michelle Scurr,[1,2] Pei X. Er,[1,2] Ker S. Tan,[1,2] Rebecca Sutton,[1,2] Feroz Ahmad,[1,2] Ritika Saxena,[1,2,3] Alexander Maytum,[1,2,3] Declan L. Turner,[1,2,3] Holly K. Voges,[1,2,3] Hieu T. Nim,[1,2,3] Kira X. Sun,[4] Bicheng Yang,[4] Nick L. Li,[4] Gareth Ball,[3,5] Andrew G. Elefanty,[1,2,3] Shireen R. Lamandé,[1,2,3] Kynan T. Lawlor,[1,2,3] Jessica M. Vanslambrouck,[1,2,3] Richard J. Mills,[1,2,3,6] Elizabeth S. Ng,[1,2,3] Edouard G. Stanley,[1,2,3] Rhiannon B. Werder,[1,2,3] Melissa H. Little,[1,2,3,7] David A. Elliott,[1,2,3,8,9,*] Enzo R. Porrello,[1,2,3,9,10,*] Maree C. Faux,[1,3,11,*] David D. Eisenstat,[1,3,12,*] Silvia Velasco,[1,2,3,*] Fernando J. Rossello,[1,2,8,13,16,*] and Mirana Ramialison[1,2,3,14,*]

[1]Stem Cell Medicine Theme, Murdoch Children's Research Institute, Parkville, VIC, Australia
[2]The Novo Nordisk Foundation Center for Stem Cell Medicine, reNEW Melbourne, Murdoch Children's Research Institute, Parkville, VIC, Australia
[3]Department of Paediatrics, University of Melbourne, Parkville, VIC, Australia
[4]BGI Australia, Brisbane, QLD, Australia
[5]Developmental Imaging, Murdoch Children's Research Institute, Parkville, VIC, Australia
[6]School of Biomedical Sciences, Queensland University of Technology, Brisbane, QLD, Australia
[7]The Novo Nordisk Foundation Center for Stem Cell Medicine, reNEW Copenhagen, University of Copenhagen, Copenhagen, Denmark
[8]Australian Regenerative Medicine Institute, Monash University, Melbourne, VIC, Australia
[9]Melbourne Centre for Cardiovascular Genomics and Regenerative Medicine, Melbourne, VIC, Australia
[10]Department of Anatomy and Physiology, School of Biomedical Sciences, The University of Melbourne, Melbourne, VIC, Australia
[11]Department of Surgery, The University of Melbourne, Parkville, VIC, Australia
[12]The Royal Children's Hospital, Parkville, VIC, Australia
[13]Department of Clinical Pathology, University of Melbourne, Melbourne, VIC, Australia
[14]Systems Biology Institute, Clayton, VIC, Australia
[15]These authors contributed equally
[16]Lead contact
*Correspondence: david.elliot@mcri.edu.au (D.A.E.), enzo.porello@mcri.edu.au (E.R.P.), maree.faux@mcri.edu.au (M.C.F.), david.eisenstat@mcri.edu.au (D.D.E.), silvia.velasco@mcri.edu.au (S.V.), fernando.rossello@mcri.edu.au (F.J.R.), mirana.ramialison@mcri.edu.au (M.R.)
https://doi.org/10.1016/j.isci.2026.115827

SUMMARY

Stem cell-derived organoids hold promise to model tissue-specific diseases. To enable this, it is crucial to assess how transcriptional signatures, cellular organization, and composition of organoids compare to *in vivo* counterparts. However, spatial transcriptomics has been challenging to apply to organoids to elucidate regional molecular identity. This study presents the first systematic profiling of multiple stem cell-derived organoid models (brain, heart muscle, heart valve, kidney, lung, cartilage, and hematopoietic) with stereo-seq, a full transcriptome, spatial assay using on-chip *in situ* RNA capture. It describes assay optimization for characterization, use of multiple organoid samples on a single chip, assesses limitations in RNA capture efficiency compared to reference tissues. Furthermore, it introduces a bespoke analysis method that partitions samples into regions for characterization. These findings inform future works to characterize organoids using spatial transcriptomics, providing insights into optimizing RNA capture of multiple organoids across a chip and regional analysis.

INTRODUCTION

Pluripotent stem cell (PSC)-derived organoid models are used to investigate human development and disease pathogenesis and provide a platform to measure drug response.[1] This requires organoids to accurately recapitulate the corresponding *in vivo* tissue, both physiologically and in cellular composition, by replicating *in vitro* the process of native stem cell development and organization.[2,3]

Spatial transcriptomics (ST) technologies capture gene expression across tissues while maintaining the anatomical and morphological structure. ST encompasses a wide array of technologies that are divided into imaging- and sequencing-based assays.[4] This study focuses on the application of

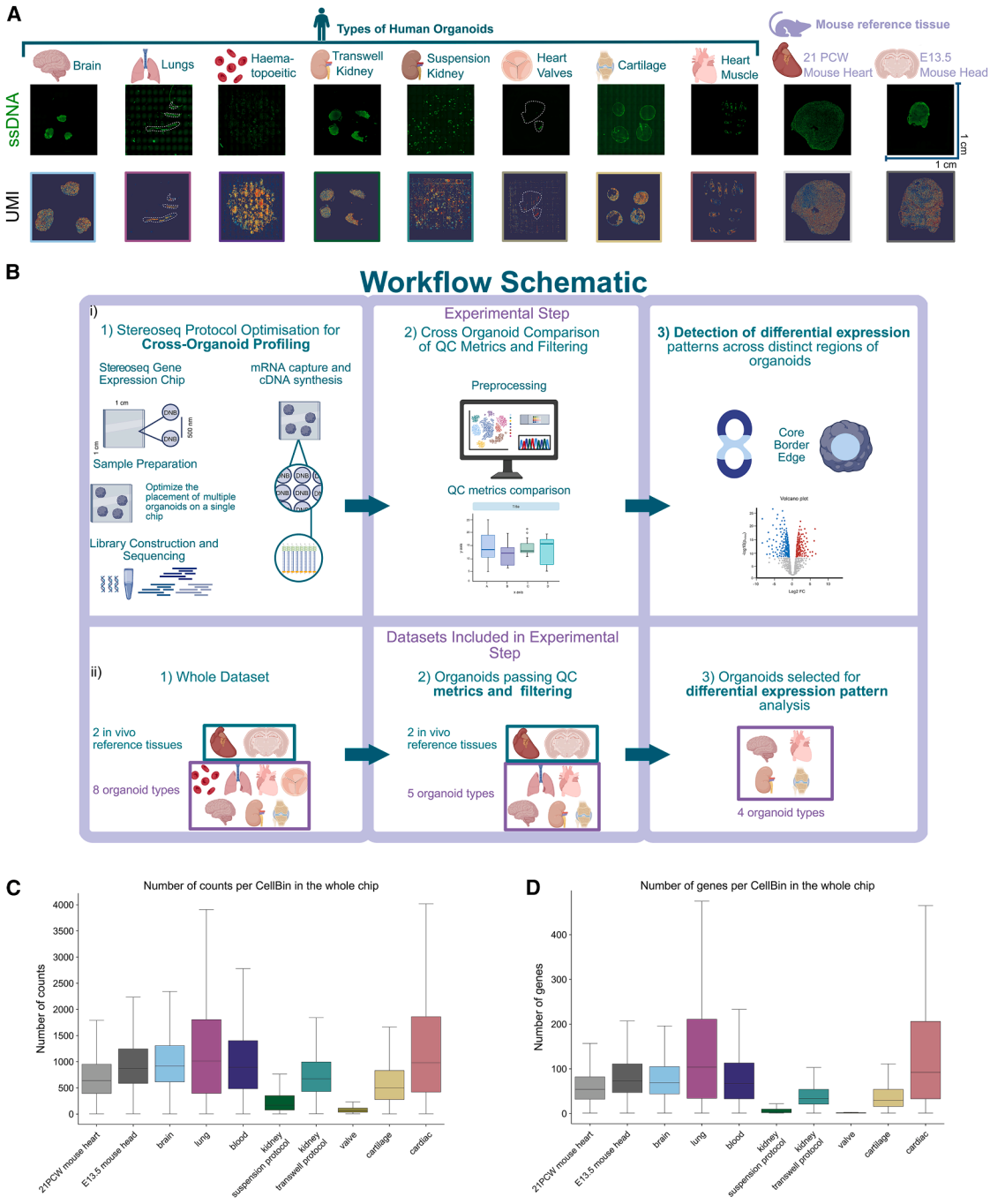

Figure 1. Overview of quality metrics across multiple organoid types and *in vivo* reference tissues when captured using the stereo-seq platform

(A) Schematic of organoid models and *in vivo* reference tissues included on individual stereo-seq 1 cm^2 chips. Immunofluorescence images display regions of ssDNA capture across the chip, while accompanying areas of high-count expression are visualized as UMI heatmaps. White dotted lines indicate organoid boundaries on UMI heatmaps and immunofluorescence images.

(B) Schematic of experimental design. (1) Steps included from sample preparation and optimization through to data analysis and investigation of regional patterns. (2) Outline of datasets included in each experimental step. Protocol optimization and cross-organoid profiling were performed on a total of 10 stereo-seq chips, divided across two *in vivo* reference tissues and eight organoid types. (3) After assessing chips that passed quality control filters, both *in vivo* reference tissues and five organoid types were retained for analysis. Finally, four organoid models were selected for region-specific analysis patterns of gene expression.

(legend continued on next page)

stereo-seq, a sequencing-based technology capable of capturing transcriptome-wide gene expression at single-cell resolution.[5] Stereo-seq profiles an embedded tissue section using a specialized chip, which allows mRNA capture and imaging simultaneously. Given the high cost of ST experiments per sample, finding a cost-effective approach to profile multiple organoids using a single chip is critical. While ST has previously been applied to a single type of organoid being placed on a stereo-seq chip,[6–8] technical challenges arise when using small-sized organoids that cover a limited portion of the ST chip. This may result in artificially lower mRNA levels or the capture of fewer gene transcripts, defined as the total data capture throughout this article. To date, there are no studies that directly compare mRNA expression and gene profiling of organoids against *in vivo* tissue. Furthermore, the placement of several individual organoids on a single chip has proven to be viable for certain organoid types,[7] yet studies describing the feasibility and benefits of simultaneous placement of multiple organoid conditions on the same chip are limited.

This study performed a systematic spatial transcriptome profiling of multiple organoid models (brain, heart muscle, heart valve, kidney, lung, cartilage, and hematopoietic), using the stereo-seq platform compared to two *in vivo* reference tissues—E13.5 mouse head tissue and 21 post-conception week (PCW) mouse heart tissue. The study describes the successful placement of multiple organoids of the same tissue type—cultured under different conditions for certain tissues—on the same chip. Subsequently, the platform's capability to clearly distinguish transcriptional gene signatures from these different individual organoids on the same stereo-seq chip was tested. The effect of size, shape, and cell type composition of different organoids on data capture, when compared to one another and to larger, *in vivo* reference E13.5 mouse head and 21 PCW mouse heart tissues was investigated. Finally, despite challenges in cell type annotation linked to challenges in achieving single-cell resolution, this study illustrates an effective analysis for uncovering region-specific differences across organoids as an alternative to cell clustering and classification. This approach enables the identification of spatially resolved biologically relevant gene expression patterns across multiple organoid models.

RESULTS

Quality evaluation of stereo-seq capture across multiple organoid types and *in vivo* reference tissues

This study systematically profiled the transcriptome of eight human organoid models (brain, lung, hematopoietic, transwell kidney, suspension kidney, heart valve, cartilage, and heart muscle), using the stereo-seq platform. A modified stereo-seq workflow was designed to capture multiple conditions where multiple organoids of the same tissue type were co-embedded and placed on a single stereo-seq chip (see STAR Methods) (Figure 1A). To prevent tissue detachment from the chip surface, as observed in cartilage, heart muscle, and kidney organoids, stereo-seq chips were coated with poly-L-lysine, as part of our modified stereo-seq workflow. To limit transcript diffusion and allow for accurate spatial gene expression profiling, tissue-specific cell permeabilization also required optimization. This optimization was critical to allow processing of multiple organoid samples, derived from the same tissue and different culture conditions on the same chip. Hematopoietic and suspension kidney organoid samples displayed higher levels of transcript diffusion, as revealed by transcripts captured outside of tissue locations, despite optimized permeabilization conditions (Figure 1A).

Two reference tissues (E13.5 mouse head and 21 PCW mouse heart) were also profiled using the standard stereo-seq workflow, with the aim to use these datasets as baselines against the characterized organoid models (Figure 1A). To account for the custom stereo-seq workflow and compensate for the differences in RNA capture across organoids, a custom bioinformatics workflow was developed, including a region-specific analysis, described in detail below (Figure 1B). This workflow filtered out low-quality organoid samples to ensure comparisons to baseline were only drawn for models for which the protocol optimization had been successful. This then allowed investigation of the increased chip coverage on data capture to determine compatibility of the stereo-seq platform with multiple organoid models. RNA capture quality across the entire chip was then assessed through a variety of metrics: comparison of the number of captured counts and genes on a per cell bin basis (Figures S1C and S1D), captured DNA nanoballs and unique reads (Figures S1A and S1B), and sequencing saturation (Figure S1C). Firstly, data capture was evaluated on cell bins (equivalent to single cells visualized across the corresponding immunofluorescence ssDNA image), and the smallest analytical unit generated during pre-processing via default cell-segmentation methods on the accompanying immunofluorescence image (ssDNA, Figure 1A). Although a large variation persisted in the total number of transcripts captured between organoids and *in vivo* tissue reference (Figures S1A and S1B), capture ranges for both the number of genes and counts per cell bin were found to be comparable across organoid models and *in vivo* reference tissues (Figures 1C and 1D), irrespective of sequencing saturation. It is worth noting that only kidney suspension organoids did not reach a saturation of 80% (Figure S1C). This suggests that the observed variation could have been introduced by differences in chip coverage area, rather than organoid type, emphasized by a positive correlation between total Unique molecular identifiers (UMIs) passing quality control (QC) and tissue size of organoid samples compared to *in vivo* reference tissue (Figure S1D).

The heart valve and kidney suspension protocol models showed a reduced RNA capture relative to other organoid models, evidenced by a low number of DNA nanoballs captured under tissue along with low numbers of mapped unique reads (Figures S1A and S1B). Additionally, the hematopoietic organoid

(C) Number of UMIs per cell bin across each chip. Data are represented as box plots, where the center line indicates the median, the box shows the interquartile range (IQR) (25th–75th percentile), and whiskers extend to 1.5× IQR.
(D) Number of genes per cell bin across each chip. Data are represented as box plots, where the center line indicates the median, the box shows the IQR, and whiskers extend to 1.5× IQR.

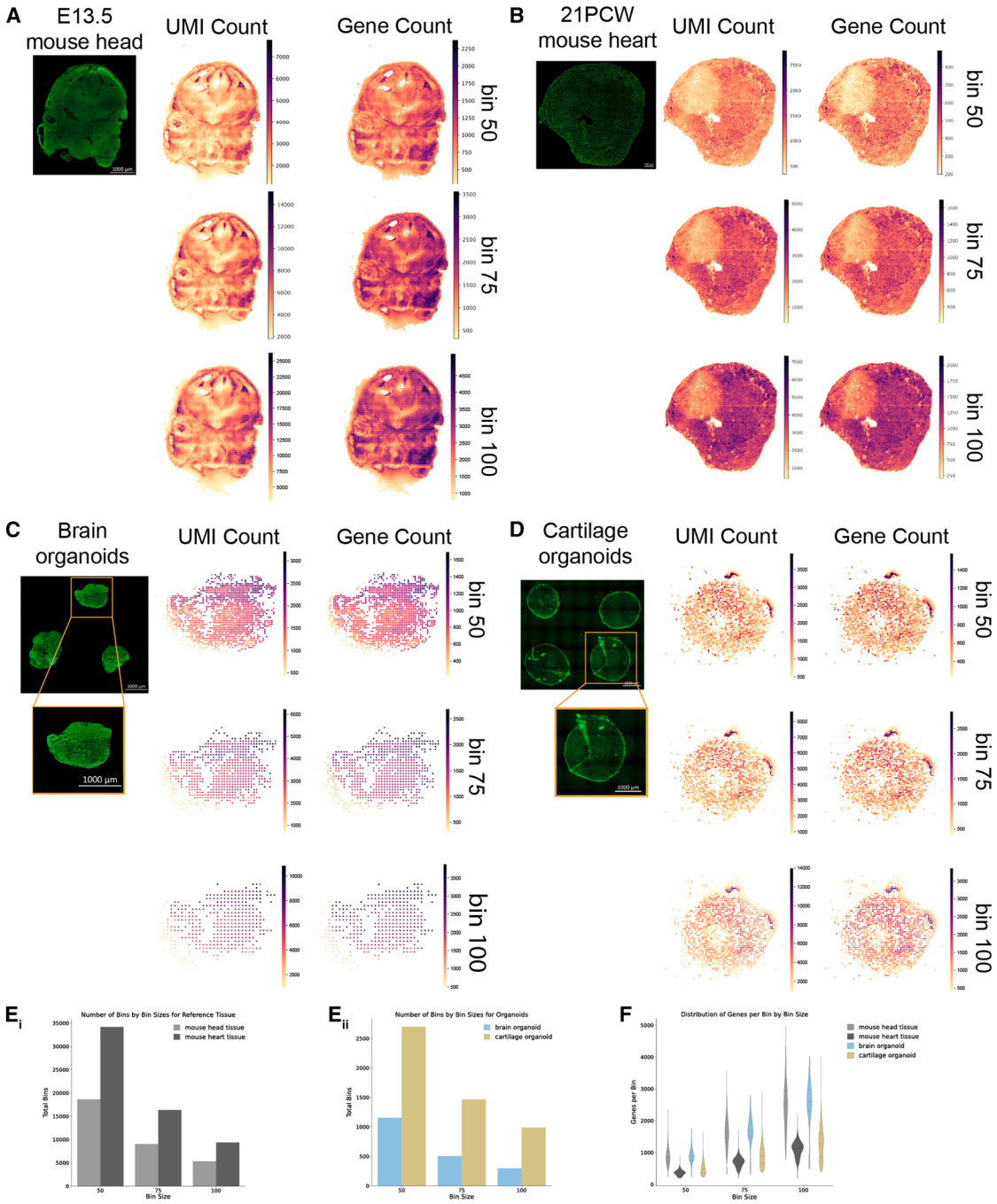

Figure 2. Effect of increasing bin size (50, 75, and 100) on spatial patterning and data visualization across *in vivo* reference tissues and organoids

(A) Immunofluorescence image of ssDNA capture and heatmaps visualizing regions of high counts and genes per bin across *in vivo* reference tissue E13.5 mouse head at increasing bin sizes.

(B) Immunofluorescence image of ssDNA capture and heatmaps visualizing regions of counts and genes per bin across *in vivo* reference tissue 21 PCW mouse heart tissue at increasing bin sizes.

(C) Immunofluorescence image of ssDNA capture and heatmaps visualizing regions of counts and genes per bin across a single brain organoid at increasing bin sizes. Brain organoid 1 displayed in the heatmaps is highlighted in the immunofluorescence image.

(D) Immunofluorescence image of ssDNA capture and heatmaps visualizing regions of counts and genes per bin across a single pseudo-replicate of cartilage organoid. Cartilage organoid 1 displayed in the heatmaps is highlighted in the immunofluorescence image.

(legend continued on next page)

chips displayed an unexpectedly broad data capture range (Figures S1A and S1B). This was likely due to the placement of a large number of organoids per chip leading to increased transcript diffusion, mainly evidenced by the presence of UMIs outside tissue regions of ssDNA (Figure 1A). Given these issues, downstream analyses focused on organoid models with uniform size and shape, resulting in an increased RNA capture across chips. Individual brain, transwell kidney, and cartilage organoid samples placed on the same chip showed comparable numbers of genes and transcripts captured compared to E13.5 mouse head and 21 PCW mouse heart *in vivo* references (Figures S1E–S1I). For quality assurance, the percentages of cell bins expressing the housekeeping genes *GAPDH*/*Gapdh* and *ACTB*/*Actb* across *in vivo* references and individual brain and cartilage organoid samples were investigated (Figure S2A). While cell-to-cell expression levels of housekeeping genes varied (Figure S2C), similar to previously reported single-cell RNA sequencing (scRNA-seq) experiments,[9] no clear spatial expression patterns of *GAPDH*/*Gapdh* and *ACTB*/*Actb* across the organoids passing QC filtering (Figures S2A–S2C) were observed, reflecting the expected homogenous expression nature of these genes. These observations also revealed no systematic differences introduced by coating chips with poly-L-lysine (Figure S2C).

Effect of increasing the spatial aggregation level on spatial patterning and data visualization across *in vivo* reference tissues and organoids

In addition to cell bin segmentation, stereo-seq experiments can also be analyzed using an aggregation-based approach (“square bin”) by grouping adjacent transcript capture areas together. Given the smaller size of the organoids compared to mouse reference tissues and RNA capture variability across all profiled tissues (Figure 1), the effect of increasing bin size on capture of RNA levels, genes, and biological signal was explored next (Figure 2). The effects of altering square bin size, which determines the resolution of defined regions, revealed loss of tissue coverage at larger bin sizes, which could further reveal differences in platform performance when profiling *in vivo* reference tissues and organoid models (Figures 2A–2D). For both *in vivo* references and different organoid models, when the bin size was increased from 50 to 75, the expected accompanying proportional decrease in the number of bins passing QC was not observed (Figures 2Ei and 2Eii).

Our analysis demonstrated that increasing the bin size from 50 to 75 to 100 (25, 37.5, and 50 μm^2, respectively)—accompanied by analysis using bespoke filtering parameters to eliminate inclusion of background signal—changes the overall tissue coverage area in both the *in vivo* reference tissues and brain and cartilage organoids at larger bin sizes (Figure 2; Table S1). However, due to the reduced size of organoid samples in general, this loss of largely peripheral signal may contribute to downstream challenges to identify cell type compositions in the organoids.

It is expected that a bin size increase of 50% would produce a 50% decrease in the number of bins. In both *in vivo* reference tissues, increasing the bin size by 50% led to a decrease in the number of bins by more than half, while a doubling of bin size led to only about one-third of the total number of bins being retained (Figure 2Ei; Table S1). In mouse head tissue, this created a drop from 18,634 bins at bin size 50 to 9,024 bins at bin size 75 and 5,313 bins at bin size 100 (Table S1). This disproportionate reduction in the number of bins with increasing bin size was more noticeable across organoids compared to *in vivo* reference tissues (Figure 2Eii; Table S1). For the brain organoids, bin size 50 resulted in a tissue area of 67,450 μm^2 being analyzed, and this fell to 49,350 μm^2 with analysis performed at bin size 100 (Table S1). We also found that larger bin sizes necessitated stricter filtering parameters to eliminate the inclusion of background signal in the tissue region, leading to removal of certain tissue areas for downstream analysis and resulting in fewer bins (Table S1). These asymmetrical changes were mirrored in the total calculated tissue area at different bin sizes for both *in vivo* reference tissues and organoid models (Table S1). In addition, increasing the bin size across organoid and reference tissues led to changes in the range of number of genes captured per bin (Figure 2F), with the range of distribution number of captured genes increasing as bin size increased.

Overall, RNA capture proved more effective at smaller bin sizes while minimizing background signal across the aforementioned tissues. Additionally, smaller bin sizes allowed for maximum tissue area to be included in downstream analysis without the addition of background noise to the dataset in both *in vivo* reference and organoid tissues. However, the relatively low number of captured UMIs and genes across individual samples, either with cell bins or a square bin size of 50 above (Figures 1C and 1D), hindered analysis at a single-cell resolution using this platform (Figures 2C and 2D).

To further investigate the feasibility of multi-sample placement on single chips, the effect of normalizing samples across the entire chip was compared to a sample-specific normalization, performed independently on samples after sub-setting (Figure S3). Overall, the spatial expression of housekeeping (*GAPDH* and *ACTB*) or organoid marker genes remained unaffected across both normalization methods (Figure S3). Evidence that normalization did not skew biological signals is reflected in the expected homogeneous expression of *COL2A1*, *COL9A3*, and *SPARC* across cartilage organoids, given that they are composed almost exclusively of chondrocyte cells (Figure S3).

Analysis of differentially expressed genes across different regions of the organoids

Despite increasing bin sizes and normalization, data generated from organoid experiments did not allow for cell clustering and further cell type classification, primarily due to insufficient capture of cell type defining transcripts and genes. This was contrasted with the clear and accurate spatial profiles of the *in vivo*

(E) Bar plots of the total number of bins captured across tissue at different bin sizes. (i) *In vivo* reference E13.5 mouse head and 21 PCW mouse heart tissue. (ii) Brain organoid 1 and cartilage organoid 1. Bars represent counts.

(F) Distribution of the number of genes captured in each bin at bin sizes 50, 75, and 100 for *in vivo* reference E13.5 mouse head, 21 PCW mouse heart, brain organoid 1, and cartilage organoid 1. Data are represented as violin plots, where the width of each violin reflects the data density.

samples (Figures S2B–S2D). Therefore, an alternative, exploratory analysis method that considers organoid regions was developed. This approach allows comparison of gene expression profiles between border and core regions of organoids, a valuable analysis given previous findings observing region-specific transcriptional differences within organoids[1,10,11] (Figure 3A).

After removing outliers (bins falling outside of the organoid boundaries), our approach classified remaining bins into inner and outer regions, based on their distance from the center of the organoid (see STAR Methods). Gene expression from bins within each region is then aggregated using a pseudo-bulk strategy, resulting in a stronger signal that overcomes the low expression of individual bins. We selected brain, transwell kidney, and cartilage organoids for this analysis on the basis of comparable shape and size of organoid samples of the same tissue type, which allowed benchmarking of the developed region-specific analysis method (Figures 3 and S4A–S4I).

The initial quality-filtering step measured the distance from each bin located at the extremes of the organoid boundaries to its *k* nearest neighboring bins and removed those that were isolated from the rest. This method successfully excluded any low-quality regions (based on UMI counts) that potentially arose from inconsistent tissue adherence to the chip (Figures 3A–3C and S4A–S4F). From this analysis, brain and cartilage organoid samples exhibited fewer outliers than those of the kidney, likely due to their uniform shape and lesser number of detached cells at the edge of the organoids (Figures S4D–S4F). This analysis subsequently enabled the identification of edge, border, and core regions within the assessed organoid models (Figures 3D and S4G–S4I). A differential expression analysis between the core and border regions of organoid models, using a pseudo-bulk analysis and organoid samples as replicates, followed. It should be noted that this approach does not account for spatially variable gene expression. In cartilage organoids, no differentially expressed genes (DEGs) were identified between these regions, confirming the homogenous cell population expected in this model[12] (Figure S4J). In contrast, brain organoids showed transcriptional differences between the border or core regions, with 13 genes differentially upregulated in core regions and 13 genes in border regions (Figure 3E). Gene set enrichment analysis (GSEA) of biological processes showed that border regions of these organoids were enriched for gene sets related to ATP synthesis and electron transport (Figure 3F), whereas core regions were enriched for gene sets related to glycolysis (Figure 3G). These observations align with those of previous studies showing enrichment of glycolytic gene sets in cortical neural progenitors which are located at the core of brain organoid,[13] while more energy-demanding neuronal populations are found at the borders of organoids at this developmental stage.[13] These findings demonstrated that the proposed region-specific approach allowed the identification of spatially and metabolically distinct cell populations in brain organoid models, which was also observed when using a Slide-seq assay, an alternative sequencing ST technique.[13]

Analysis of DEGs across different organoids within a specific region

We further expanded the use of our method to irregularly shaped heart muscle organoids. These organoids had a ‘‘figure eight’’ shape, with two pole regions on either side of the organoid and a center region, amenable to measurement contractile functions[14] (Figures 4A and 4B). Heart muscle organoids were cultured under two different conditions, using a previously published standard serum-free method (control)[15] and a directed maturation method (DM) for enhanced maturation and contractile force[16] (Figures 4A and 4B). By applying the developed region-specific analysis, pole regions were filtered out from downstream analysis due to low cell density and mRNA capture (Figures 4A and 4B). This shows that this method could act as a secondary quality control based on tissue distribution. Center regions of the control and DM organoids were compared using organoid samples as replicates (Figures 4B and S4K–S4L), showing transcriptional differences between the compared conditions (Figure 4C). This analysis identified an upregulation of MRPS12, a mitochondrial riboprotein, in the DM-cultured organoids (Figure 4D), suggesting a difference in mitochondrial activity in organoid culture in DM media. In control heart muscle organoids, the GSEA identified enriched gene sets implicated in ion channel activities (Figure 4E), while gene sets linked to mitochondrial activities, ATP synthesis, and metabolism were upregulated in DM heart muscle organoids (Figure 4F). Enrichment of these gene sets reflects recent findings that reported alternative usage of ion channels and increase in sarcomere maturity of organoids cultured in DM media indicated through the downregulation of ion channel genes and upregulation of metabolic genes, respectively.[16] The transcriptional differences captured through ST between serum-free control and DM heart muscle organoids resemble previous characterization of these models, demonstrating the validity of ST assays to capture transcriptional differences of organoids grown under different conditions.

DISCUSSION

This study assessed the performance of stereo-seq, an ST by sequencing assay, in eight induced pluripotent stem cell (iPSC)-derived human organoid models and two mouse *in vivo* tissue references. The main objective was to validate this technology across multiple organoid tissue types in comparison to reference tissues, in which spatial gene expression profiles showed anatomical specificity at single-cell resolution.

Across the eight organoid models assessed, cartilage, brain, and transwell kidney organoids resulted in sample quality comparable to tissue references, which could be attributed to their size and relatively uniform, round shapes. Despite this, RNA capture of these samples failed to achieve single-cell gene expression resolution. Organoids with smaller surface areas, such as suspension kidney and hematopoietic organoids (notwithstanding comparable transcript capture and total gene counts) displayed high amounts of diffuse gene expression captured outside the organoid surfaces. We suspect this was likely due to additional challenges presented by these organoids, cultured in more of a ‘‘liquid-phase’’ compared to other tissue types, resulting in transcript diffusion. Another challenge in applying stereo-seq to these organoids was their lack of adhesiveness, likely contributing to non-uniform transcript capture across chips. As a remedy, poly-L-lysine chip coating was used to maximize tissue adhesion (see STAR Methods). The data generated from heart

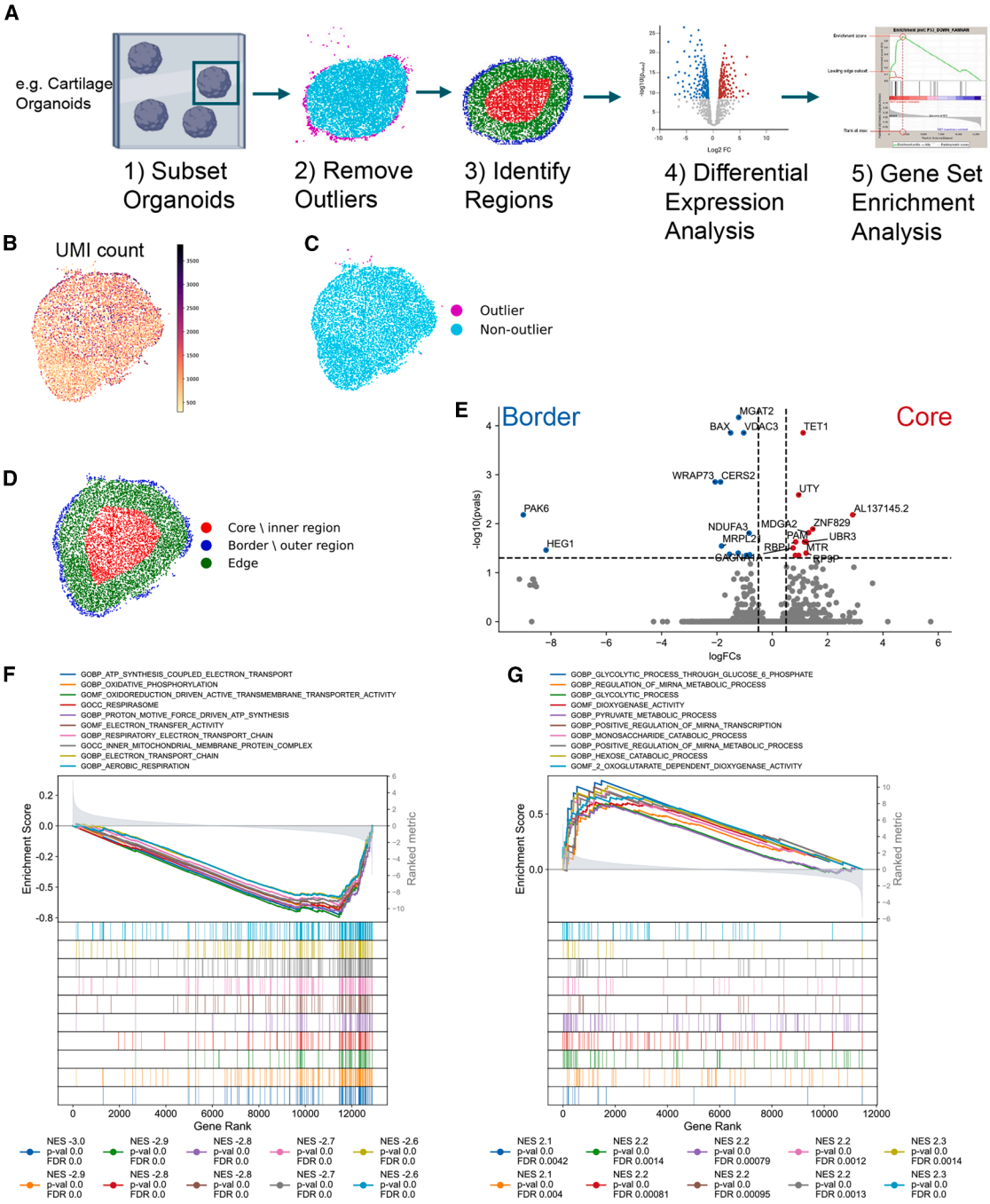

Figure 3. Analysis of spatially restricted, differentially expressed genes across center and border regions

(A) Schematic of representative workflow of region-specific analysis between core and border regions, demonstrated using cartilage organoids.

(B) Heatmap of regions of UMI counts across brain organoid 1, using cell bins.

(C) Outlier cell bins identified and visualized in magenta across brain organoid 1, representing a false-positive signal to be removed before region analysis.

(D) Edge (green), border (blue), and center (red) regions highlighted for analysis in brain organoid 1.

(E) Volcano plots of genes upregulated in core region (visualized in red) and those upregulated in border region (visualized in blue) for brain organoid pseudo-replicates 1–4.

(F) Gene set enrichment analysis output showing top 10 negatively enriched terms in core of brain organoids. Each curve represents the enrichment profile of the gene set. Legend annotations include normalized enrichment score, *p* value, and FDR q value.

(G) Gene set enrichment analysis output showing top 10 positively enriched terms in core of brain organoids.

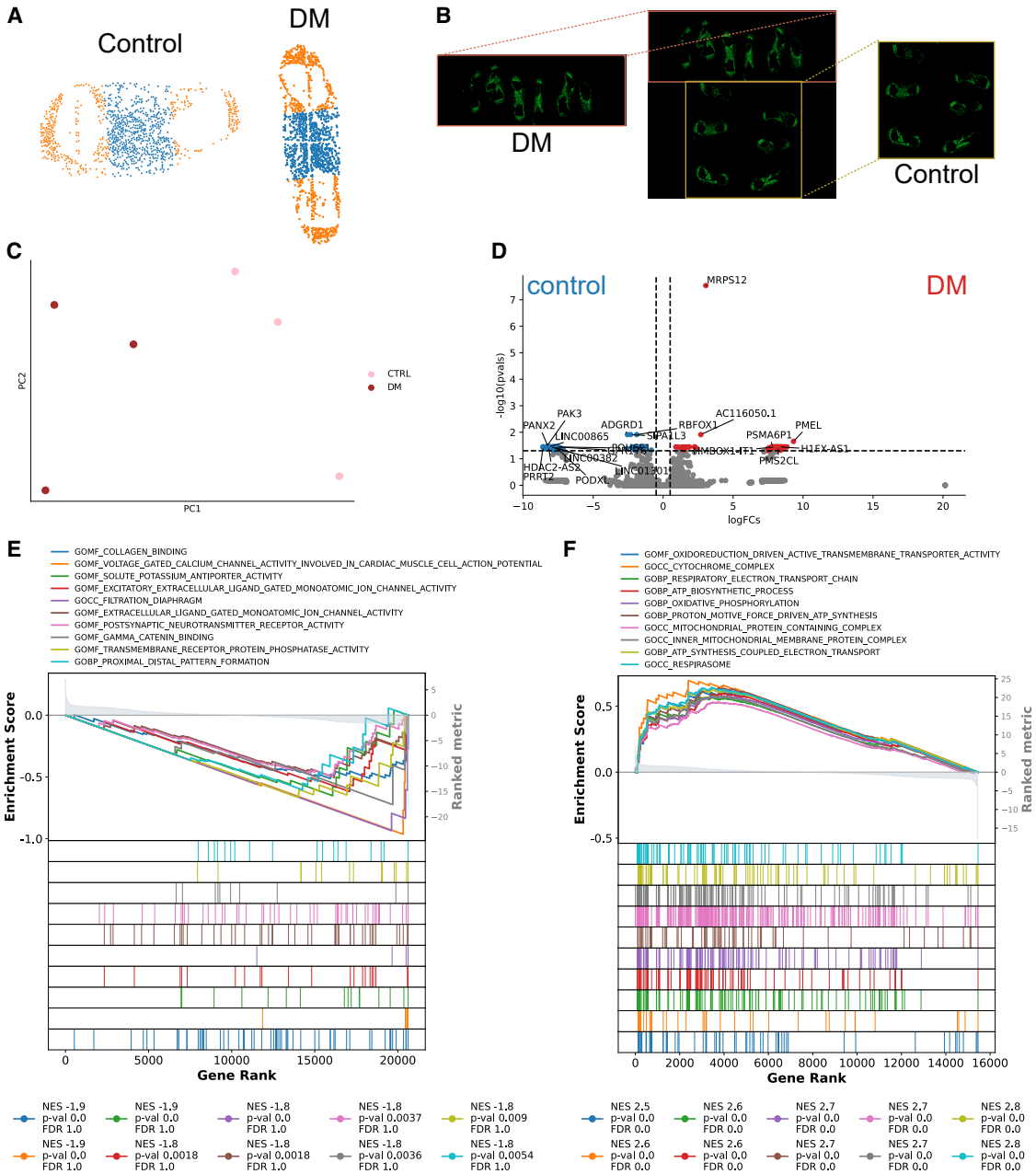

Figure 4. Analysis of differentially expressed genes across center regions of heart muscle organoids of different conditions

(A) Example of outlined center (blue) and pole (orange) regions across DM and control heart muscle organoids.

(B) Overview of immunofluorescent heart muscle organoids across stereo-seq chip outlining the placement of six DM organoids on the top and six control organoids on the bottom side of the chip.

(C) PCA plot of data from 3 center regions of control organoids and 3 regions of DM organoids.

(D) Volcano plots of genes upregulated in center of 3 DM organoids (red) compared to genes upregulated in center of 3 control organoids (blue).

(E) Gene set enrichment analysis showing top enriched terms in the center of control heart muscle organoids.

(G) Gene set enrichment analysis showing top enriched terms in the center of DM heart muscle organoids.

muscle organoids demonstrated that this method was effective in improving organoid adhesion and should be considered for all organoids to improve data quality.

This study tested the feasibility of placing multi-sample placement on a single chip. Previously, ST technology required single tissue sections to be placed on separate chips to yield optimal outcomes.[7,8] Our analysis revealed that placing up to 12 sections on the same chip, as in the case of heart muscle organoids, still resulted in accurate transcript capture, both cultured in the same media, and organoids grown in different culture media,

such as the case of control vs. DM heart muscle organoids. The ability to maximize coverage with multiple sections per chip greatly extends the potential use of ST technology for organoids, ensuring high data value per chip and reduced inter-chip variability.

The expression of housekeeping genes such as *GAPDH* and *ACTB* was uniform across cartilage, brain, and transwell kidney organoids, although only in less than 50% of the identified cell bins, resembling expression patterns of these genes in *in vivo* reference tissues. However, the identification of region-specific transcriptional signatures in organoids was limited when using cell bins (i.e., single-cell resolution), likely due to the relatively low number of transcripts and genes captured per cell bin. While the number of transcripts and genes detected per bin was comparable to those in other studies utilizing stereo-seq,[5] it was found to be lower than the accepted range for scRNA-seq experiments. Interestingly, increasing square bin sizes, at the expense of losing single-cell resolution, did not resolve the challenges in detecting region-specific expression patterns in organoids models. This may also be a product of the unbiased transcript capture technology coupled with a low number of transcripts captured, leading to an overrepresentation of abundant transcripts. This shows that while whole-transcriptome ST, including stereo-seq and Visium HD, could capture transcripts from organoid models, its utility for identifying region-specific expression patterns at single-cell level in these model systems was limited. However, this higher-throughput approach for characterization of organoids could be useful for discerning spatially distinct molecular signatures, as previously shown to be viable using *in vivo* tissue samples signatures.[5,17]

Given the smaller size of organoids compared to *in vivo* tissue, the structural compartments in these models could be relatively subtle and marked by fewer cells. Coupled with the challenge of achieving single-cell resolution, this hindered the ability of ST technique in capturing spatially resolved gene expression in organoids and, hence, the identification of defined patterning. The use of cryo-sections may also limit the assessment of these organoids, as structural compartments could be rare and difficult to capture on a single-cell-thick layer. These challenges demonstrate the need to further optimize protocols to apply ST to organoid models. As mentioned above, improvements could include applying alternative chip coating methods to further increase tissue adhesion or organoid fixation to better preserve spatial gene expression profiles.

As standard clustering and cell type classification approaches could not be applied to dataset from organoids of this study, we developed an alternative, exploratory regional analysis method that allowed spatial gene expression profiling in organoids between core and border regions. We demonstrated its power in identifying region-specific biological processes as well as its utility as a secondary quality control filter when applied to brain and heart muscle organoids. Given the use of Euclidean distance to calculate outliers, the application of this analysis as a secondary quality control filter to round organoids enables more accurate calculation of cells that have detached from main organoid bodies. As mentioned, the ability to understand region-specific gene expression patterns in these models could be key to elucidating general structural organization that may be present in these systems. This knowledge could then be used to further advance organoid models to better reflect their *in vivo* counterparts, especially with regards to progressing organoid patterning for the study of developmental tissue patterning. This could have significant implications in developmental biology, such as identifying processes of cell differentiation. As ST platforms for RNA capture continue to evolve and expand imaging options, an updated stereo-seq protocol incorporating H&E imaging, a morphology-based analysis, could be incorporated into future analytical pipelines.

Overall, this study explores the use of profiling multiple organoid types using ST platform. It demonstrates the feasibility of placing multiple organoids generated under different culture conditions on a single stereo-seq chip, allowing capture of distinct biological signatures from each model. Furthermore, we illustrate the abilities and limitations of profiling a range of organoid types with the current stereo-seq platform, identifying potential steps for future optimization, such as the use of poly-L-lysine for adhesion. Given the limitation around current RNA capture in allowing organoid-specific cell type annotation, which is not mitigated by increasing bin size for analysis, we developed a regional-specific analysis workflow for capturing biologically relevant gene expression. This provides a basis for future optimization of organoid profiling using the stereo-seq platform, including maximizing data capture from a single experiment.

Limitations of the study

Although the application of stereo-seq ST technology across a wide range of organoids was examined, other ST technologies may present different outcomes when applied to organoid systems. For instance, other sequencing-based ST technology such as 10× Visium HD, also offers spatial gene expression profiling at single-cell resolution, and, given the different chemistry and transcript capture technology, it could produce alternative results.[18] Alternatively, probe-based imaging ST technologies could also perform differently, with sub-cellular resolution and higher specificity. To validate findings reported in this study, traditionally spatial gene expression profiling methods such *in situ* hybridization or immunofluorescence could be performed to assess the accuracy of the gene expression patterns identified. Additionally, expanding the range of *in vivo* tissues to correspond to the organoid systems included, such as including mouse kidney and lung tissues, would provide additional points of reference to validate the use of stereo-seq ST technology on various organ and organoid systems.

RESOURCE AVAILABILITY

Lead contact

Requests for further information and resources should be directed to and will be fulfilled by the lead contact, Fernando Rossello (fernando.rossello@mcri.edu.au).

Materials availability

This study did not generate new unique reagents. All materials used are commercially available or previously published.

Data and code availability

- The datasets generated during this study are available in Gene Expression Omnibus (GEO) under accession number GEO: GSE294759.

- All original code is available on GitHub at https://github.com/Ramialison-Lab/StereoseqOrganoids.
- Any additional information required to reanalyze the data reported in this paper is available from the lead contact upon request.

ACKNOWLEDGMENTS

This work was supported by the Novo Nordisk Foundation Center for Stem Cell Medicine, reNEW, supported by Novo Nordisk Foundation grant number NNF21CC0073729; a BGI STOmics Grant to N.C. and M.R. E.R.P. is supported by an Investigator Grant from the National Health and Medical Research Council (NHMRC) of Australia (GNT2008376). S.V. is supported by an Investigator Grant from the NHMRC of Australia (GNT2025776) and a Fellowship from the Sarah and Lachlan Murdoch Foundation. H.K.V. was supported by a Postdoctoral Fellowship (106645) from the National Heart Foundation of Australia. M.R. is funded by a Future Leader Fellowship (107328) from the Heart Foundation of Australia, a Human Frontiers Science Program Grant (RGP008/2024). M.R. and H.T.N. are supported by an NHMRC Ideas Grant (APP1180905). Additional infrastructure funding to the Murdoch Children's Research Institute was provided by the Australian Government National Health and Medical Research Council Independent Research Institute Infrastructure Support Scheme. The Australian Regenerative Medicine Institute is supported by grants from the State Government of Victoria and the Australian Government.

AUTHOR CONTRIBUTIONS

Conceptualization, M.R.N., N.C., R.F.L., and M.R.; methodology, M.R.N., N.C., R.F.L., and M.R.; software, M.R.N.; formal analysis, M.R.N.; investigation, M.R.N., N.C., R.F.L., A.L., L.R., R.S., A.M., M.S., N.K.T., V.S., D.L.T., M.W., P.X.E., K.S.T., R.S., F.A., H.K.V., and H.T.N.; resources, K.X.S., B.Y., and B.L.L.; data curation, M.R.N., N.C., and R.F.L.; writing – original draft, M.R.N., N.C., R.F.L., F.J.R., and M.R.; writing – review & editing, all authors; supervision, S.V., G.B., M.C.F., D.D.E., F.J.R., M.R., D.A.E., E.R.P., and R.J.M.; funding acquisition, N.C., M.R., A.G.E., S.R.L., K.T.L., J.M.V., R.J.M., E.S.N., E.G.S., R.B.W., M.H.L., D.A.E., E.R.P., H.K.V., M.C.F., D.D.E., and S.V.

DECLARATION OF INTERESTS

H.K.V. is a co-inventor on a patent held by the Murdoch Children's Research Institute that relates to stem cell derivation of valve cells and tissues. E.R.P. and R.J.M. are co-inventors on patents related to cardiac organoid maturation and cardiac therapeutics and are co-founders, scientific advisors, and stockholders in Dynomics. F.J.R. receives institutional and salary support as (1) a co-investigator and subcontractor with the Peter MacCallum Cancer Center for an investigator-initiated trial, which receives funding support from Regeneron Pharmaceuticals, and (2) a co-investigator on a translational research project funded by a Regeneron Pharmaceuticals grant.

STAR★METHODS

Detailed methods are provided in the online version of this paper and include the following:

- KEY RESOURCES TABLE
- EXPERIMENTAL MODEL AND STUDY PARTICIPANT DETAILS
  - Animal maintenance and ethics approval
  - IPSCs maintenance and ethics approval
  - Organoids generation
- METHOD DETAILS
  - Stereo-seq T-chip coating
  - Sample processing and library preparation
  - Bioinformatics workflow
- QUANTIFICATION AND STATISTICAL ANALYSIS

SUPPLEMENTAL INFORMATION

Supplemental information can be found online at https://doi.org/10.1016/j.isci.2026.115827.

Received: December 19, 2025
Revised: January 19, 2026
Accepted: April 16, 2026
Published: April 21, 2026

REFERENCES

1. Zhao, D., Lei, W., and Hu, S. (2021). Cardiac organoid - a promising perspective of preclinical model. Stem Cell Res. Ther. *12*, 272. https://doi.org/10.1186/s13287-021-02340-7.
2. Prasad, M., Kumar, R., Buragohain, L., Kumari, A., and Ghosh, M. (2021). Organoid Technology: A Reliable Developmental Biology Tool for Organ-Specific Nanotoxicity Evaluation. Front. Cell Dev. Biol. *9*, 696668. https://doi.org/10.3389/fcell.2021.696668.
3. Zhao, Z., Chen, X., Dowbaj, A.M., Sljukic, A., Bratlie, K., Lin, L., Fong, E.L.S., Balachander, G.M., Chen, Z., Soragni, A., et al. (2022). Organoids. Nat. Rev. Methods Primers *2*, 94. https://doi.org/10.1038/s43586-022-00174-y.
4. Waylen, L.N., Nim, H.T., Martelotto, L.G., and Ramialison, M. (2020). From whole-mount to single-cell spatial assessment of gene expression in 3D. Commun. Biol. *3*, 602. https://doi.org/10.1038/s42003-020-01341-1.
5. Chen, A., Liao, S., Cheng, M., Ma, K., Wu, L., Lai, Y., Qiu, X., Yang, J., Xu, J., Hao, S., et al. (2022). Spatiotemporal transcriptomic atlas of mouse organogenesis using DNA nanoball-patterned arrays. Cell *185*, 1777–1792.e21. https://doi.org/10.1016/j.cell.2022.04.003.
6. Chiaradia, I., Imaz-Rosshandler, I., Nilges, B.S., Boulanger, J., Pellegrini, L., Das, R., Kashikar, N.D., and Lancaster, M.A. (2023). Tissue morphology influences the temporal program of human brain organoid development. Cell Stem Cell *30*, 1351–1367.e10. https://doi.org/10.1016/j.stem.2023.09.003.
7. Ma, S., Wang, W., Zhou, J., Liao, S., Hai, C., Hou, Y., Zhou, Z., Wang, Z., Su, Y., Zhu, Y., et al. (2024). Lamination-based organoid spatially resolved transcriptomics technique for primary lung and liver organoid characterization. Proc. Natl. Acad. Sci. USA *121*, e2408939121. https://doi.org/10.1073/pnas.2408939121.
8. Wahle, P., Brancati, G., Harmel, C., He, Z., Gut, G., Del Castillo, J.S., Xavier da Silveira Dos Santos, A., Yu, Q., Noser, P., Fleck, J.S., et al. (2023). Multimodal spatiotemporal phenotyping of human retinal organoid development. Nat. Biotechnol. *41*, 1765–1775. https://doi.org/10.1038/s41587-023-01747-2.
9. Lin, Y., Ghazanfar, S., Strbenac, D., Wang, A., Patrick, E., Lin, D.M., Speed, T., Yang, J.Y.H., and Yang, P. (2019). Evaluating stably expressed genes in single cells. GigaScience *8*, giz106. https://doi.org/10.1093/gigascience/giz106.
10. Hautefort, I., Poletti, M., Papp, D., and Korcsmaros, T. (2022). Everything You Always Wanted to Know About Organoid-Based Models (and Never Dared to Ask). Cell. Mol. Gastroenterol. Hepatol. *14*, 311–331. https://doi.org/10.1016/j.jcmgh.2022.04.012.
11. Moss, S.P., Bakirci, E., and Feinberg, A.W. (2025). Engineering the 3D structure of organoids. Stem Cell Rep. *20*, 102379. https://doi.org/10.1016/j.stemcr.2024.11.009.
12. Lamandé, S.R., Ng, E.S., Cameron, T.L., Kung, L.H.W., Sampurno, L., Rowley, L., Lilianty, J., Patria, Y.N., Stenta, T., Hanssen, E., et al. (2023). Modeling human skeletal development using human pluripotent stem cells. Proc. Natl. Acad. Sci. USA *120*, e2211510120. https://doi.org/10.1073/pnas.2211510120.
13. Uzquiano, A., Kedaigle, A.J., Pigoni, M., Paulsen, B., Adiconis, X., Kim, K., Faits, T., Nagaraja, S., Antón-Bolaños, N., Gerhardinger, C., et al. (2022). Proper acquisition of cell class identity in organoids allows definition of

fate specification programs of the human cerebral cortex. Cell *185*, 3770–3788.e27. https://doi.org/10.1016/j.cell.2022.09.010.

14. Mills, R.J., Titmarsh, D.M., Koenig, X., Parker, B.L., Ryall, J.G., Quaife-Ryan, G.A., Voges, H.K., Hodson, M.P., Ferguson, C., Drowley, L., et al. (2017). Functional screening in human cardiac organoids reveals a metabolic mechanism for cardiomyocyte cell cycle arrest. Proc. Natl. Acad. Sci. USA *114*, E8372–E8381. https://doi.org/10.1073/pnas.1707316114.
15. Voges, H.K., Foster, S.R., Reynolds, L., Parker, B.L., Devilée, L., Quaife-Ryan, G.A., Fortuna, P.R.J., Mathieson, E., Fitzsimmons, R., Lor, M., et al. (2023). Vascular cells improve functionality of human cardiac organoids. Cell Rep. *42*, 112322. https://doi.org/10.1016/j.celrep.2023.112322.
16. Pocock, M.W., Reid, J.D., Robinson, H.R., Charitakis, N., Krycer, J.R., Foster, S.R., Fitzsimmons, R.L., Lor, M., Devilée, L.A.C., Batho, C.A.P., et al. (2025). Maturation of human cardiac organoids enables complex disease modeling and drug discovery. Nat. Cardiovasc. Res. *4*, 821–840. https://doi.org/10.1038/s44161-025-00669-3.
17. Xie, P., Shen, J., Yang, Y., Wang, X., Liu, W., Cao, H., Zheng, Y., Wu, C., Mao, G., Chen, L., et al. (2025). Digital reconstruction of full embryos during early mouse organogenesis. Cell *188*, 4754–4772.e18. https://doi.org/10.1016/j.cell.2025.05.035.
18. Oliveira, M.F.d., Romero, J.P., Chung, M., Williams, S.R., Gottscho, A.D., Gupta, A., Pilipauskas, S.E., Mohabbat, S., Raman, N., Sukovich, D.J., et al. (2025). High-definition spatial transcriptomic profiling of immune cell populations in colorectal cancer. Nat. Genet. *57*, 1512–1523. https://doi.org/10.1038/s41588-025-02193-3.
19. Vlahos, K., Sourris, K., Mayberry, R., McDonald, P., Bruveris, F.F., Schiesser, J.V., Bozaoglu, K., Lockhart, P.J., Stanley, E.G., and Elefanty, A.G. (2019). Generation of iPSC lines from peripheral blood mononuclear cells from 5 healthy adults. Stem Cell Res. *34*, 101380. https://doi.org/10.1016/j.scr.2018.101380.
20. Vanslambrouck, J.M., Wilson, S.B., Tan, K.S., Soo, J.Y.C., Scurr, M., Spijker, H.S., Starks, L.T., Neilson, A., Cui, X., Jain, S., et al. (2019). A Toolbox to Characterize Human Induced Pluripotent Stem Cell-Derived Kidney Cell Types and Organoids. J. Am. Soc. Nephrol. *30*, 1811–1823. https://doi.org/10.1681/ASN.2019030303.
21. Werder, R.B., Liu, T., Abo, K.M., Lindstrom-Vautrin, J., Villacorta-Martin, C., Huang, J., Hinds, A., Boyer, N., Bullitt, E., Liesa, M., et al. (2022). CRISPR interference interrogation of COPD GWAS genes reveals the functional significance of desmoplakin in iPSC-derived alveolar epithelial cells. Sci. Adv. *8*, eabo6566. https://doi.org/10.1126/sciadv.abo6566.
22. Lilianty, J., Bateman, J.F., and Lamandé, S.R. (2021). Generation of a heterozygous COL2A1 (p.G1113C) hypochondrogenesis mutation iPSC line, MCRIi019-A-7, using CRISPR/Cas9 gene editing. Stem Cell Res. *56*, 102515. https://doi.org/10.1016/j.scr.2021.102515.
23. Palla, G., Spitzer, H., Klein, M., Fischer, D., Schaar, A.C., Kuemmerle, L.B., Rybakov, S., Ibarra, I.L., Holmberg, O., Virshup, I., et al. (2022). Squidpy: a scalable framework for spatial omics analysis. Nat. Methods *19*, 171–178. https://doi.org/10.1038/s41592-021-01358-2.
24. Pedregosa, F. (2011). Scikit-learn: Machine learning in Python. J. Mach. Learn. Res. *12*, 2825. https://doi.org/10.1145/2786984.2786995.
25. Muzellec, B., Teleńczuk, M., Cabeli, V., and Andreux, M. (2023). PyDESeq2: a python package for bulk RNA-seq differential expression analysis. Bioinformatics *39*, btad547. https://doi.org/10.1093/bioinformatics/btad547.
26. Badia-I-Mompel, P., Vélez Santiago, J., Braunger, J., Geiss, C., Dimitrov, D., Müller-Dott, S., Taus, P., Dugourd, A., Holland, C.H., Ramirez Flores, R.O., and Saez-Rodriguez, J. (2022). decoupleR: ensemble of computational methods to infer biological activities from omics data. Bioinform. Adv. *2*, vbac016. https://doi.org/10.1093/bioadv/vbac016.
27. Fang, Z., Liu, X., and Peltz, G. (2023). GSEApy: a comprehensive package for performing gene set enrichment analysis in Python. Bioinformatics *39*, btac757. https://doi.org/10.1093/bioinformatics/btac757.
28. Yammine, K.M., Mirda Abularach, S., Sampurno, L., Bateman, J.F., Lamandé, S.R., and Shoulders, M.D. (2023). Using CRISPR/Cas9 to generate a heterozygous COL2A1 p.R719C iPSC line (MCRIi019-A-6) model of human precocious osteoarthritis. Stem Cell Res. *67*, 103020. https://doi.org/10.1016/j.scr.2023.103020.
29. Abo, K.M., Sainz de Aja, J., Lindstrom-Vautrin, J., Alysandratos, K.D., Richards, A., Garcia-de-Alba, C., Huang, J., Hix, O.T., Werder, R.B., Bullitt, E., et al. (2022). Air-liquid interface culture promotes maturation and allows environmental exposure of pluripotent stem cell-derived alveolar epithelium. JCI Insight *7*, e155589. https://doi.org/10.1172/jci.insight.155589.
30. Hawkins, F.J., Suzuki, S., Beermann, M.L., Barillà, C., Wang, R., Villacorta-Martin, C., Berical, A., Jean, J.C., Le Suer, J., Matte, T., et al. (2021). Derivation of Airway Basal Stem Cells from Human Pluripotent Stem Cells. Cell Stem Cell *28*, 79–95.e8. https://doi.org/10.1016/j.stem.2020.09.017.
31. Jacob, A., Morley, M., Hawkins, F., McCauley, K.B., Jean, J.C., Heins, H., Na, C.L., Weaver, T.E., Vedaie, M., Hurley, K., et al. (2017). Differentiation of Human Pluripotent Stem Cells into Functional Lung Alveolar Epithelial Cells. Cell Stem Cell *21*, 472–488.e10. https://doi.org/10.1016/j.stem.2017.08.014.
32. Ng, E.S., Sarila, G., Li, J.Y., Edirisinghe, H.S., Saxena, R., Sun, S., Bruveris, F.F., Labonne, T., Sleebs, N., Maytum, A., et al. (2025). Long-term engrafting multilineage hematopoietic cells differentiated from human induced pluripotent stem cells. Nat. Biotechnol. *43*, 1274–1287. https://doi.org/10.1038/s41587-024-02360-7.
33. Voges, H.K., Mills, R.J., Porrello, E.R., and Hudson, J.E. (2023). Generation of vascularized human cardiac organoids for 3D in vitro modeling. STAR Protoc. *4*, 102371. https://doi.org/10.1016/j.xpro.2023.102371.
34. Lawlor, K.T., Vanslambrouck, J.M., Higgins, J.W., Chambon, A., Bishard, K., Arndt, D., Er, P.X., Wilson, S.B., Howden, S.E., Tan, K.S., et al. (2021). Cellular extrusion bioprinting improves kidney organoid reproducibility and conformation. Nat. Mater. *20*, 260–271. https://doi.org/10.1038/s41563-020-00853-9.
35. Kumar, S.V., Er, P.X., Lawlor, K.T., Motazedian, A., Scurr, M., Ghobrial, I., Combes, A.N., Zappia, L., Oshlack, A., Stanley, E.G., and Little, M.H. (2019). Kidney micro-organoids in suspension culture as a scalable source of human pluripotent stem cell-derived kidney cells. Development *146*, dev172361. https://doi.org/10.1242/dev.172361.
36. Velasco, S., Kedaigle, A.J., Simmons, S.K., Nash, A., Rocha, M., Quadrato, G., Paulsen, B., Nguyen, L., Adiconis, X., Regev, A., et al. (2019). Individual brain organoids reproducibly form cell diversity of the human cerebral cortex. Nature *570*, 523–527. https://doi.org/10.1038/s41586-019-1289-x.
37. Huang, J., Hume, A.J., Abo, K.M., Werder, R.B., Villacorta-Martin, C., Alysandratos, K.D., Beermann, M.L., Simone-Roach, C., Lindstrom-Vautrin, J., Olejnik, J., et al. (2020). SARS-CoV-2 Infection of Pluripotent Stem Cell-Derived Human Lung Alveolar Type 2 Cells Elicits a Rapid Epithelial-Intrinsic Inflammatory Response. Cell Stem Cell *27*, 962–973.e7. https://doi.org/10.1016/j.stem.2020.09.013.
38. Gong, C., Li, S., Wang, L., Zhao, F., Fang, S., Yuan, D., Zhao, Z., He, Q., Li, M., Liu, W., et al. (2024). SAW: an efficient and accurate data analysis workflow for Stereo-seq spatial transcriptomics. GigaByte *2024*, gigabyte111. https://doi.org/10.46471/gigabyte.111.
39. Fang, S., Xu, M., Cao, L., Liu, X., Bezulj, M., Tan, L., Yuan, Z., Li, Y., Xia, T., Guo, L., et al. (2025). Stereopy: modeling comparative and spatiotemporal cellular heterogeneity via multi-sample spatial transcriptomics. Nat. Commun. *16*, 3741. https://doi.org/10.1038/s41467-025-58079-9.

STAR★METHODS

KEY RESOURCES TABLE

REAGENT or RESOURCE	SOURCE	IDENTIFIER
Deposited data		
Raw data	This paper	GEO: GSE294759
Homo sapiens reference genome (GRCh38)	Genome Reference Consortium	https://www.ncbi.nlm.nih.gov/grc/human
Mus musculus reference genome (GRCm39)	Genome Reference Consortium	https://www.ncbi.nlm.nih.gov/grc/mouse
Experimental models: Cell lines		
Haematopoietic organoids derived from PB001.1 iPSCs (male) clone #1	MCRI (Vlahos et al.[19])	MCRIi001-A
Transwell kidney organoid derived from CRL1502.2 iPSCs (female)	MCRI (Vanslambrouck et al.[20]) https://hpscreg.eu/cell-line/MCRIi019-A	MCRIi019-A
Suspension kidney organoid derived from MAFBmTagBFP:GATA3mCherry reporter iPSCs (male)	MCRI (Vanslambrouck et al.[20]) https://pcen.wustl.edu/items/request-ipsc-cell-lines/	RID: 14-3QDG
Brain organoids derived from PB001.1 (male), PB001.1 harbouring a heterozygous 1bp insertion at chr5:177,135,105 (c.2insG) and from PB001.1 harbouring a homozygous 4bp deletion at chr5:177,135,106 (c.3_6delGGAT)	MCRI (Vlahos et al.[19])	MCRIi001-A
Heart organoid derived from PB10.5 iPSCs (male)	MCRI (Vlahos et al.[19])	MCRIi010-A (RRID:CVCL_UK91)
Lung organoids derived from BU3 NGST CRISPRi iPSCs (male)	MCRI (Werder et al.[21])	Werder et al.[21] https://doi.org/10.1126/sciadv.abo6566
Cartilage organoids derived from MCRIi019-A iPSCs (female)	MCRI (Lilianty et al.[22])	MCRIi019-A-7
Experimental models: Organisms/strains		
Wild-type mouse – Strain name: Crl:CD1(ICR) -Elite	Charles River Laboratory	#022
Wild-type mouse - Strain name: Tg(Myh6-Tpm1*E54K)67Dfw	Jackson Laboratories	035610
Software and algorithms		
ImageStudio v2.1.1	BGI Genomics	https://www.stomics.tech
SAW v6.12	BGI Genomics	https://github.com/STOmics/SAW
Squidpy v1.2.2	Palla et al.[23]	https://github.com/scverse/squidpy
Stereopy v1.2.3	BGI Genomics	https://github.com/STOmics/Stereopy
Python v3.8.2	Python Software Foundation	https://www.python.org
scikit-learn v1.5.0	Pedregosa et al.[24]	https://github.com/scikit-learn/scikit-learn
PyDESeq2 v1.6.0	Muzellec et al.[25]	https://github.com/owkin/PyDESeq2
decoupler v0.4.11	Badia-i-Mompel et al.[26]	https://github.com/saezlab/decoupler
GSEApy v1.0	Fang et al.[27]	https://github.com/zqfang/GSEApy
Other		
Scripts and code	This paper	https://github.com/Ramialison-640 Lab/StereoseqOrganoids

EXPERIMENTAL MODEL AND STUDY PARTICIPANT DETAILS

Animal maintenance and ethics approval

All animals were housed in the Murdoch Children's Research Institute (MCRI) Disease Model Unit and all animal works performed were conducted under the approval and in compliance of the MCRI Animal Ethics Committee agreements (SPPL20327). Timed pregnant mice were sacrificed by cervical dislocation following MCRI AEC approved protocols at embryonic day 13.5 where the presence of a vaginal plug after mating indicated (E0.5). E13.5 mouse heads and 21 postconceptional week (PCW) mouse hearts were fresh

frozen in OCT (SAKURA Cat# 4583) and stored at -800C until further processing. The mouse from which the heart sample was obtained was male, whereas the sex of the mouse from which the head sample was derived could not be determined.

IPSCs maintenance and ethics approval

PB001.1 induced pluripotent stem cells (iPSCs) (male)[19] were used for haematopoietic organoid differentiation, CRL1502.2 iPSCs (female)[20] were used for transwell kidney organoid differentiation, MAFBmTagBFP:GATA3mCherry reporter iPSCs[20] were used for suspension kidney organoid differentiation, PB10.5 iPSCs (male)[19] were used for heart organoid differentiation. Brain organoids were generated from PB001.1,[19] PB001.1 harbouring a heterozygous 1bp insertion at chr5:177,135,105 (c.2insG) and PB001.1 harbouring a homozygous 4bp deletion at chr5:177,135,106 (c.3_6delGGAT). BU3 NGST CRISPRi iPSCs (male)[21] were used for lung organoid differentiation. MCRIi019-A iPSCs (female)[22] were used for cartilage organoid differentiation.[28] Mycoplasma contamination in all iPSCs were monitored and excluded by regular testing. Karyotyping of all iPSCs were performed regularly and no significant genomic imbalances were identified.

All iPSCs, with the exception of those used for brain organoids were grown on human embryonic stem cell (hESC)-qualified Matrigel Matrix (Corning Cat# 354277), with varying medium conditions. iPSCs for brain organoids were grown on Geltrex™ LDEV-Free Reduced Growth Factor Basement Membrane Matrix (Thermo Fisher Scientific Cat # A1413301). iPSCs used for differentiation of cartilage, transwell kidney, suspension kidney, and haematopoietic organoids were maintained in Essential 8 Medium (Thermo fisher Scientific Cat# A1517001). iPSCs used for lung organoid differentiations were maintained in StemFlex Medium (Thermo Fisher Scientific Cat# A3349401), whereas iPSCs for brain and heart organoid differentiation were maintained in mTESR1 Medium (Stem Cell Technologies Cat# 85857).

Ethical approval for the generation and/or use of human iPSCs were obtained from MCRI and Boston University and were carried out in accordance with the National Health and Medical Research Council of Australia (NHMRC) regulations. iPSCs studies were approved by The Royal Children's Hospital Human Research Ethics Committee (references 33001A and 93025).

Organoids generation

Eight organoid models were generated in accordance to previously described differentiation protocols, including lung airway and alveolar type 2 organoids[29–31] haematopoietic organoids,[32] heart organoids serum-free controls[14,15,33] heart organoids with directed maturation (DM),[34] cartilage organoids,[12] heart valve organoids,[33] transwell kidney organoids,[34] suspension kidney organoids,[35] and brain organoids.[13,36] Specifically, following alterations were included in respective organoids to generate different experimental conditions. Both iPSC-derived lung organoids at air-liquid interface were infected on the apical surface with respiratory syncytial virus (RSV-A2, MOI 1) as previously described for SARS-CoV-2.[37] After 4 hours, the inoculum was removed and cells washed. Uninfected and infected samples were collected 72 hours post infection. Both were at day 114 of differentiation when plated at ALI and infected 13 days post airlift. From day 48, cartilage organoids were either grown without additional treatment for 14 days or treated as follows. Condition 1: cartilage organoids were cultured without additional treatment after day 48 for 7 days followed by addition of 10nM Triiodothyronine (Sigma Aldrich Cat# T6397) for 7 days, condition 2: cartilage organoids were cultured without additional treatment after day 48 for 7 days, followed by 7 days in osteogenic medium[12] and condition 3: cartilage organoids were grown with addition of 10nM Triiodothyronine for 7 days followed by 7 days in osteogenic medium. All cartilage organoid conditions were harvested at day 62. Blood organoids were harvested at day 10. Brain organoids grown from all three cell lines were collected on day 31. The suspension kidney organoids were collected after 7 days of monolayer and 11 days in 3D culture. The cardiac organoids were collected after 15 days in 2D culture ad 14 days and 3D.

METHOD DETAILS

Stereo-seq T-chip coating

At the time of harvest, organoids were separated from culturing media and washed in PBS, then placed in pre-chilled OCT. Organoids were then transferred to plastic mould containing OCT, and frozen in an ethanol or isopropanol slurry. For brain organoids, three organoids were embedded together and placed on the chip, whereas four transwell kidney, and cartilage organoids were embedded together and placed on the same chip. Eighteen heart valve organoids were embedded together and placed on the same chip. Six heart organoids of each condition (serum-free and DM) were embedded together in an array of 12 organoids. Over 20 haematopoietic and suspension kidney organoids were embedded in a single mould. For lung organoids, a pair of airway and alveolar type 2 sections, either infected or non-infected, were embedded in OCT together. However, the uninfected airway section was lost during sample processing, resulting in only infected airway section present and alveolar type 2 sections remained.

Sample processing and library preparation

For the heart muscle, heart valve, and cartilage organoids, the sections were mounted on poly-L-lysine coated Stereo-seq T-chip to enhance adhesion. Stereo-seq T-chips were washed using nuclease-free H2O twice and dried, then coated with 100μL of 0.01% (w/v) poly-L-lysine (Sigma Aldrich Cat# P8920) for 10 minutes at room temperature. Post incubation, the chips were washed with nuclease-free H2O twice and dried on a 37°C slide dryer.

Samples were prepared and processed using the STOmics Transcriptomics kit (STOmics Cat# 111KT114) in accordance with manufacturer's instructions (BGI stereo-seq Transcriptomics set for Chip-on-a-slide user manual version B) with slight variations. 10μm sections of mouse tissue samples including E13.5 heads and 21PCW hearts, brain organoids, kidney organoids, lung organoids, and haematopoietic organoids were cryo-sectioned on CM3050S cryostat (Leica) and mounted on room temperature T-chips, then processed according to the STOmics user manual. 10μm cryo-sections of cartilage, heart muscle, and heart valve organoids were placed on room temperature poly-L-lysine coated stereo-seq T-chips, then processed according to the STOmics user manual. All cryo-sections were fixed in ice cold methanol for 30 minutes at -30°C. Tissue section permeabilization times were as follows: lung, haematopoietic, transwell kidney, suspension kidney, and cartilage organoid sections were permeabilised for 12 minutes, mouse head and brain organoids for 15 minutes, heart organoids and engineered heart valves for 18 minutes, and mouse heart for 24 minutes. The cDNA purification and library preparation of each sample was constructed using the STOmics library preparation kit (STOmics Cat# 111KL114) in accordance with manufacturer's instructions (BGI STOmics stereo-seq Transcriptomics set for Chip-on-a-slide user manual version B). Quality of the final cDNA library size was assessed using D1000 Tapestation Reagent (Agilent Technologies Cat# 5067-5602) and Screentape (Agilent Technologies Cat# 5067-5582) and the concentration measured with Qubit dsDNA HS kit (Thermo Fisher Scientific Cat# Q33231). The sequencing of the libraries was performed at the BGI Oceanic headquarters using MGI DNBSEQ T7 sequencer, with 1260 million reads targeted recovery per sample.

Bioinformatics workflow

Preprocessing

The stitched .czi files taken with the Z2 Axio Imager were processed through ImageStudio v. 2.1.1 using the ssDNA setting for staining to ensure they passed QC. They were then transformed into .ipr . files to ensure compatibility with the SAW[38] pipeline. The paired FASTQ, mask and transformed .ipr files were then processed using the SAW pipeline v.6.12[38] using default parameters including cell binning. Raw FASTQ files generated from mouse hearts were aligned using default SAW mapping parameters to the reference genome GRCm39 while raw FASTQ files generated from organoids were aligned to the reference genome GRCh38.

All organoids and *in vivo* reference tissues was conducted using the Squidpy package v1.2.2[23] and Stereopy package v1.2[39] with Python v3.8.2.

Evaluation of quality metrics

Quality metrics were evaluated globally across the whole chip for each organoid type, and at the individual-organoid level for organoids of interest. Number of counts and number of genes per chip were computed using Stereopy, while number of mapped reads, mRNA-captured DNA nanoballs under tissue and sequencing saturation values were extracted from SAW output files and report. Per-organoid metrics were computed after filtering the data to retain only a single organoid, using the coordinates extracted with the with the plt.interact_spatial_scatter() function of Stereopy. This analysis was repeated for 3 different bin sizes (50, 75 and 100). Before computing the number of bins, genes and counts, a filtering was applied to remove signal outside of the organoid boundaries and bins with extremely low counts or high mitochondrial gene percentage. This filtering ensured that we counted and evaluated only bins representing true biological signal. The filtering criteria varied between kinds of organoids and tissues as it was highly dependent on the specific counts' distribution. In some case, poor-quality bins were not limited to clear outliers but represented a substantial part of the distribution, making outlier-based filtering inadequate. The specific filtering steps are documented in the code associated with the publication.

Organoid-specific regional analysis

Artifacts and outliers at the edge of the organoids were first filtered to retain biologically relevant spatial information, as these frequently contained abnormal amount of UMIs counts (Figures 3A–3C and S4A–S4C). For each of the brain, cartilage and transwell kidney organoids (which were all largely circular in shape), we first calculated the centroid coordinates, then Euclidean distance of each point from the centroid was computed. We identified points with distances greater than the 90th percentile of all distances as ''distant points.'' Then we proceeded to detect outliers, that are points located outside the organoid represented false signals. These artifacts needed to be systematically removed to ensure that only biologically relevant spatial information was retained. These artifacts were located at a distance from the rest of the organoid cells, making it necessary to apply a targeted filtering approach. To remove outliers, we applied a k-nearest neighbours (k-NN) approach using the NearestNeighbors() function from sklearn v1.5.0[24] and ball_tree algorithm parameter. A k parameter of 10 was used for brain organoids and 250 for kidney and cartilage. Since most of the false signals were spatially distant from the organoid cells, k-NN was used to identify points with abnormally high distances to their nearest neighbours. However, to prevent central hollow regions from being misclassified as outliers, we restricted this analysis to the distant bins. For each distant bin, the average distance to its nearest neighbours was computed and standardized using a Z-score transformation. Bins with a Z-score greater than 2 (or higher depending on the specific case) were classified as outliers and subsequently removed from further analysis. (Figures 3C and S4D–S4F).

Following the removal of outliers, we computed the convex hull of the remaining bins to define the spatial boundary of the dataset. To further classify points into distinct spatial regions of the 'edge', 'border' and 'core', we calculated the minimum distance of each point to the convex hull boundary. Based on the distance distribution we classified each bin as either belonging to the: 'edge' for bins within the 10th percentile of boundary distances, 'border' for bins with distances between the edge threshold and half of the maximum distance, and 'core' for bins with distances exceeding the border threshold (Figures 3D and S4G–S4I). The 'edge' of the organoid often contained an abnormal number of counts and was removed from further analysis. After spatial classification,

we generated pseudo-bulk samples using core and border regions of individual organoids placed on the same chip and performed differential expression analysis between the core and border regions of the same organoid types. Pseudobulk was performed using the pydeseq2 v1.6.0[25] and decoupler v0.4.11[26] packages. The get_pseudobulk() function was used to generate pseudobulk samples from the anndata object using the core and border regions from each kind of organoid. This was then built into a DeSeq2 object and differential expression analysis performed. We treated the organoids on the same chip as pseudo-replicates, as even if the organoids were not exactly biological replicates but belonged to either different lines subjected to editing (brain organoids) or different growing conditions (cartilage organoids), the aim of the analysis was to identify regional differences in general within the inner and outer areas of the organoids, regardless of the organoid conditions. Subsequently, we conducted Gene Set Enrichment Analysis (GSEA) to determine enriched pathways and biological processes associated with differentially expressed genes.

For the heart organoids which had an elliptic shape, to approximate the organoid boundary, a convex hull was computed using the set of spatial coordinates. Specifically, the algorithm Quickhull was used to identify the smallest convex polygon capable of enclosing all points. Then each bin's distance to the convex hull boundary was computed by treating each bin's coordinates as a point and measuring its distance to the perimeter of the convex polygon. This metric provided an estimate of whether a bin was located near the tissue edge (small distance) or more centrally (larger distance). To remove perimeter effects and focus on interior tissue regions, bins in the lower 15th percentile of boundary distance were excluded. The remaining data (with distances above this threshold) formed the ''filtered'' subset of bins, considered representative of the tissue's interior.

The spatial coordinates of the filtered bins were then subjected to PCA. The first principal component (PC1) was assumed to capture the tissue's major ''long axis.'' This vector (PC1) was used for subsequent segmentation of the tissue into poles and centre regions. Each filtered bin was projected onto the long-axis vector by calculating a dot product between the spot's spatial coordinates and the principal-axis vector. This yielded a one-dimensional scalar value for each spot, referred to as its ''projected distance.'' The minimum and maximum projected distances defined the overall range (or ''length'') along this axis. The axis was then divided into three segments of equal length, the first segment from the minimum projection to one-third of the total range, the middle segment covering the next one-third of the range and the final segment from two-thirds of the range to the maximum projection. Bins in the bottom or top third of this range were labelled as ''pole'', whereas spots in the central third were labelled as ''centre.'' Differential expression analysis in pseudo-bulk was performed between centre of the serum free and directed maturation heart organoids.

QUANTIFICATION AND STATISTICAL ANALYSIS

GSEA was performed using GSEApy v1.0.[27] Genes were ranked based on log2 fold change from differential expression analysis. Enrichment scores were calculated using the preranked method against the Gene Ontology (GO) gene sets from the Molecular Signatures Database (MSigDB, c5.go.v2023.2.Hs.symbols.gmt). Adjusted p-values were computed using the Benjamini–Hochberg method.